

19. COMPOSITE VELOCITY PROFILE OF SHELF SITE 1103 (ODP LEG 178, WESTERN ANTARCTIC PENINSULA)¹

T. Moerz,² R. Laronga,³ C. Lauer-Leredde,⁴ C. Escutia,⁵ and
T.C.W. Wolf-Welling⁶

ABSTRACT

Site 1103 was one of a transect of three sites drilled across the Antarctic Peninsula continental shelf during Leg 178. The aim of drilling on the shelf was to determine the age of the sedimentary sequences and to ground truth previous interpretations of the depositional environment (i.e., topsets and foresets) of progradational seismostratigraphic sequences S1, S2, S3, and S4. The ultimate objective was to obtain a better understanding of the history of glacial advances and retreats in this west Antarctic margin. Drilling the topsets of the progradational wedge (0–247 m below seafloor [mbsf]), which consist of unsorted and unconsolidated materials of seismic Unit S1, was very unfavorable, resulting in very low (2.3%) core recovery. Recovery improved (34%) below 247 mbsf, corresponding to sediments of seismic Unit S3, which have a consolidated matrix. Logs were only obtained from the interval between 75 and 244 mbsf, and inconsistencies on the automatic analog picking of the signals received from the sonic log at the array and at the two other receivers prevented accurate shipboard time-depth conversions. This, in turn, limited the capacity for making seismic stratigraphic interpretations at this site and regionally.

This study is an attempt to compile all available data sources, perform quality checks, and introduce nonstandard processing techniques for the logging data obtained to arrive at a reliable and continuous depth vs. velocity profile. We defined 13 data categories using differential traveltimes information. Polynomial exclusion techniques with various orders and low-pass filtering reduced the noise of the initial data

¹Moerz, T., Laronga, R., Lauer-Leredde, C., Escutia, C., and Wolf-Welling, T.C.W., 2001. Composite velocity profile of shelf Site 1103 (ODP Leg 178, western Antarctic Peninsula). *In* Barker, P.F., Camerlenghi, A., Acton, G.D., and Ramsay, A.T.S. (Eds.), *Proc. ODP, Sci. Results*, 178, 1–34 [Online]. Available from World Wide Web:

<http://www-odp.tamu.edu/publications/178_SR/VOLUME/CHAPTERS/SR178_19.PDF>. [Cited YYYY-MM-DD]

²GEOMAR Research center for Marine Geosciences, Wisshofstrasse 1-3, C4, 24148 Kiel, Federal Republic of Germany. tmoerz@geomar.de

³Université de Montpellier II, Place Eugène Bataillon, Institut des Sciences de la Terre, de l'Eau et de l'Espace de Montpellier, Laboratoire Géophysique Tectonique Sédimentologie, cc 060, bât. 22, 34095 Montpellier Cedex 05, France.

⁴Schlumberger, 369 Tristar Drive, Webster, TX 77598, USA.

⁵Ocean Drilling Program, Texas A&M University, 1000 Discovery Drive, College Station, TX 77845, USA.

⁶Institute for Geosciences, Christian Albrechts University Kiel, Olshausenstrasse 40, 24098 Kiel, Federal Republic of Germany.

Initial receipt: 16 January 2001

Acceptance: 25 June 2001

Web publication: 28 November 2001
Ms 178SR-229

pool and produced a definite velocity depth profile that is synchronous with the resistivity logging data. A comparison of the velocity profile produced with various other logs of Site 1103 further validates the presented data. All major logging units are expressed within the new velocity data. A depth-migrated section with the new velocity data is presented together with the original time section and initial depth estimates published within the Leg 178 *Initial Reports* volume. The presented data confirms the location of the shelf unconformity at 222 ms two-way traveltime (TWT), or 243 mbsf, and allows its seismic identification as a strong negative and subsequent positive reflection.

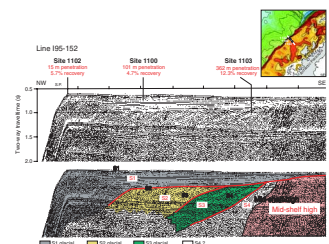
INTRODUCTION

The Antarctic shelf differs in many ways from continental shelves of mid and low latitudes and even from shelves of high northern latitudes. The Antarctic shelves in water depths between 300 and 1000 m are overdeepened and slope landward, principally because of the effect of glacial erosion and flexural loading by grounded ice (Ten Brink and Cooper, 1992; Barker et al., 1998). Sedimentary sequences exhibit two principal geometries in seismic reflection profiles collected across the West Antarctic Peninsula shelf: shelf topsets and slope foresets form the prograding wedge (Larter et al., 1994; Larter and Barker, 1989, 1991). In most areas of the middle and inner shelf, the topsets and underlying foresets are separated by a prominent regional unconformity (Larter et al., 1997). This unconformity marks a major change in the style of deposition from progradational to aggradational and progradational, adding large sediment-retaining capacities to the shelf (Fig. F1). Prograding sedimentary sequences on the continental shelf record changes in West Antarctic ice sheet volume, sea level, climate, ice and sediment-induced isostatic change, and tectonic and thermal effects.

The aim of drilling the shelf-transect Sites 1100, 1102, and 1103 during Leg 178 was to characterize the age and depositional environment of seismostratigraphic Units S1 (topsets) and S2, S3, and S4 (foresets of the prograding wedge). Unfortunately, drilling through the topset sequences was very difficult with the available rotary core barrel (RCB). Unsorted crystalline clasts (up to headsized) in an unindurated sand/silt/clay matrix prevented rapid penetration and resulted in minimal core recovery, primarily as a result of clogging of the central opening of the rotary drill bit and the core catcher with stones. Despite drilling difficulties, Site 1103 penetrated to 362.7 mbsf with mixed recoveries. The upper 247 m of cored sediment, belonging for the most part to seismic Unit S1, yielded only 2.3% recovery. The lower 116 m of cored material with a cemented matrix belonging to seismic Unit S3 yielded 34% recovery (Fig. F1). A hole blockage prevented the collection of logging data below 244 mbsf (Shipboard Scientific Party, 1999a). Thus, no or only very limited comparisons and cross-checks of log and laboratory data are possible. In our investigation, we compiled all available data sources and performed quality checks and nonstandard processing techniques with the logging data obtained to arrive at a reliable and continuous depth velocity profile presented in this paper.

Reliable velocity profiles of the shelf for time-depth conversions of multichannel seismic reflection profiles are needed for all further geological interpretations and models of shelf sedimentation in seismic sections (Camerlenghi et al., in press). Even though the shelf sediment record is less continuous and age constraints are less confined com-

F1. Location of sites drilled along a shelf transect, p. 16.



pared to all other depositional environments drilled during Leg 178 (i.e., inner continental shelf deep basins and continental rise drift deposits), the best possible depth control of the shelf sequences is essential for regional stratigraphic correlations across the Antarctic Peninsula continental shelf and between shelf and rise.

DATA RESOURCES AND METHODS

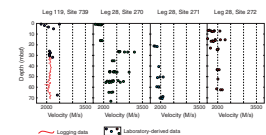
In the following chapter, the maximum drill depth of 367 mbsf reached in Hole 1103A is divided into three depth ranges: 0–70, 70–244, and 244–367 mbsf. Each depth interval is discussed separately regarding available velocity information and processing techniques used.

Interval 0–70 mbsf

The depth interval between 0 and 70 mbsf is particularly limited with regard to available velocity information and, thus, is the most speculative one. Unstable hole conditions caused the pipe to be pulled up only to 84 mbsf prior to logging. No useful logging data were obtained through the pipe over the first 75 m. Very low core recovery in this interval also prevented the collection of velocity data in the laboratory. Based on laboratory measurements on core samples recovered from Hole 1100C of the shelf transect, we measured reasonable shipboard Hamilton frame (PWS3 contact probe system) values of 1650–1700 m/s for the upper 0–3.5 mbsf (Shipboard Scientific Party, 1999b). In order to fill the remaining gap from 3.5 to 75 mbsf, all available Ocean Drilling Program (ODP) and Deep Sea Drilling Project (DSDP) velocity information was compiled from Antarctic shelf topsets (Fig. F2). For this study, we considered data of four existing drill sites depending on the availability of data, shelf geometry, location on the shelf, and reported lithology: Site 739 of ODP Leg 119 in Prydz Bay and Sites 270–272 of DSDP Leg 28 in the Ross Sea. Of all recorded shelf topset values between 5 and 75 mbsf, 92% are in the range of 1800 to 2500 m/s. The average of all recorded velocity values over this depth interval is 2172 m/s. Considering sediment descriptions and corresponding logging data given in the Leg 119 *Initial Reports* volume (Shipboard Scientific Party, 1989) and by Hambrey et al. (1991), sediments from Site 739 consist of dominantly uncemented diatom-rich diamictites with large igneous and metamorphic clasts in the upper 70 mbsf. Even though the degree of compaction may differ compared to sediments of the upper 70 mbsf of Site 1103, Leg 178, the recorded velocities are close to the overall topset values considered in our comparison (2112 m/s).

In summary, we took three velocity values from Site 1100C of the shelf transect in the depth range of 0.7–3.5 mbsf and added a velocity value of 1630 m/s at the sediment/water interface (0 mbsf). The seafloor value of 1630 m/s is based on extrapolations of the Site 1100C data mainly for ease of use in later calculations of depth-traveltime curves and synthetic seismograms. For the following interval between 3.5 and 70 mbsf, we used the average velocity (2112 m/s) of Site 739 (5–75 mbsf), ODP Leg 119, Prydz Bay. In addition to geological reasons, the decision to take Site 739 velocity values is based on the availability of logging data and the good agreement between logging and laboratory derived data for this site. Considering the introduced error, the assumptions are reasonably conservative because all known mid-shelf Antarctic

F2. Velocity data from the Prydz Bay and Ross Sea continental shelves, p. 18.



velocities of the upper 75 mbsf only show small acoustic velocity variations focused in the 1800 to 2500 m/s range.

Interval 70–244 mbsf

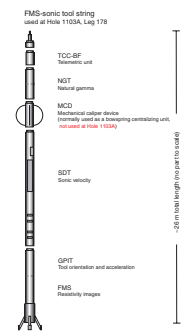
Three logging tool strings (triple combination [TC], geological high-resolution magnetic tool [GHMT], and the Formation MicroScanner [FMS]-sonic tool) were deployed at Hole 1103A. After completion of the TC logging descent, difficulties in reentering the base of the pipe resulted in the loss of the 1.5-m-long accelerator porosity sonde (APS) bow spring. In order to avoid complications with the missing parts still in the borehole, the FMS-sonic tool was used without its three centralizing bow springs of the mechanical caliper device (MCD) (Fig. F3). During two logging passes with the FMS-sonic tool (Fig. F3), transit-time and velocity information were obtained between 124 and 244 mbsf (during the first run, pass one) and from the seafloor to 243 mbsf (during the second run, pass two).

The Schlumberger sonic logging tool used at Site 1103A is commercially known as the array sonic or sonic digital tool (SDT) (Fig. F4). It carries two piezoelectric ceramic monopole transmitters that are separated by 2 ft near the downhole end of the tool. The transmitted signals have a dominant frequency of 10 kHz with a fire rate of 7.5 Hz. Ten ceramic receivers are arranged at various spacings uphole with respect to the transmitters. Two of the receivers are located in the central part of the tool, at distances of 3 and 5 ft from the upper transmitter. The remaining eight wideband receivers are clustered 6 in apart, forming an array near the top of the tool from 8 to 11.5 ft above the upper transmitter (Schlumberger, 1989). The various transmitter/receiver spacings allow the simultaneous recording of many different transit times. Detection and recording of an “analog transit time” occur in each case when the signal level at the receiver crosses a fixed threshold. This may or may not occur on the true first arrival of the signal, depending on several circumstances impacting the signal-to-noise ratio downhole. The standard output transit times with their respective transmitter/receiver spacings are listed in Table T1. A graphic representation is given in Figure F4.

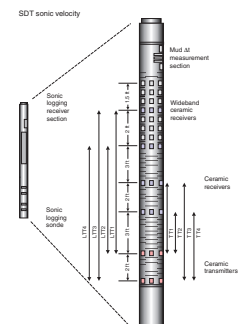
Four differential time or ΔT outputs of the logging software (Delta-T [DT] computed from TT1, TT2, and TT4; Delta-T Long [DTL] computed from TT1, TT3, and TT4; Delta-T Long Near [DTLN] computed from LTT1, LTT2, and LTT4; and Delta-T Long Far [DTLF] computed from LTT1, LTT3, and LTT4) estimate the formation slowness (inverse of velocity). Each relies on a computation combining four individual transit-time outputs. This gives an answer that is compensated against small inaccuracies resulting from tool tilt, sudden changes in hole diameter, etc. However, should a single transit time be detected incorrectly, any DT output that uses it is rendered completely invalid.

Nowhere in the logged interval were all transit times simultaneously correct. Typically, four or five of the eight were wrong at any given depth, rendering the standard formation slowness estimates completely useless. There are several reasons why this might have occurred. In general, large boreholes (>13 in) and unconsolidated formations are challenging for sonic logging because the signal is attenuated by travel through fluid and slow formation. The fundamental problem with slow formations (<2000 m/s) and the high firing frequency of 10 kHz is the resulting long wavelength with the possibility of interference of subsequent wavelets at the receivers. Additionally, the lack of the upper cen-

F3. Schematic of the FMS-sonic tool string used at Site 1103, p. 19.



F4. Drawing of transmitter and receiver configuration of the SDT sonic velocity tool, p. 20.



T1. Transmitter/receiver spacings, SDT sonic velocity tool, p. 31.

tralizing unit (MCD; Fig. F3) resulted in the tool being off center, further attenuating the signal and causing additional acoustic noise generated by the tool touching the borehole wall. Consequently, the automatic detection of the signals received at the array and at the two other receivers was inconsistent over time, and the signal was often picked within noise preceding the first true arrival (Shipboard Scientific Party, 1999b). Another reason for the recording of poor and inconsistent data could be due to strong velocity inhomogeneity within the logged formations. Tills with unlithified matrix and large clasts show large velocity differences within the measurement range of the tool. Matrix velocities may be in the range of 1800 m/s, whereas those of crystalline clasts can be as high as 5000 m/s (e.g., fig. 24 and PWS3 data for Site 1103 in Shipboard Scientific Party, 1999b). Judging from FMS image observation, large clasts of different sizes, embedded in a finer grained matrix, are unequally distributed around the borehole. Therefore, it seems possible that an emitted signal can take strongly contrasting travel paths on different sides of the borehole wall.

An additional DT output of the logging software (referred to herein as DC) is calculated using digital coherence mapping. At each 6-in (~0.15 m) sample interval, the waveforms of the eight wideband array receivers are digitized and stacked with various time offsets that compensate for moveout. The correct moveout (and formation slowness) at each depth is recognized from the offset that produces the highest amplitude stack. The data obtained are self diagnostic to some degree in that the coherency of the eight waveforms is a quantifiable indicator of confidence in the data. This technique is more robust in the difficult conditions described above, but in this case, only limited intervals featured coherent waveforms. Small-scale formation inhomogeneity may have contributed to the lack of a consistent moveout across the 3.5-ft array.

Remedial onboard processing focused individually on the widely spaced receiver/transmitter geometries LTT1 (10 ft) and LTT2 (8 ft) that showed the most consistent transit times. But this is a weak technique, considering that individual transit times do not account for traveltime within the drill slurry gap between tool and formation. A first attempt toward determining true formation velocities was to divide the transit time by the transmitter-receiver spacing and to add 10% to the resulting velocity to correct for the acoustically slower gap between tool and formation (Shipboard Scientific Party, 1999b). This method is not capable of correcting for varying borehole diameters and varying densities of the slurry within the tool/borehole gap. Additionally, the method assumes that a signal recorded in acoustically faster formations will also pass the tool/borehole gap faster than a signal recorded within acoustically slower formations. These data also have inherently poor vertical resolution determined by the transmitter-receiver spacing used.

In contrast, the data processed postcruise and presented in this paper uses exclusively differential times (ΔT), which automatically account for the tool-formation gap. Any pair of transit times of different spacing can be used to estimate formation slowness, provided that they are of different transmitter-receiver spacings. Dividing the difference in transit time by the difference in transmitter-receiver spacing, we obtain a ΔT :

$$\Delta T = (TTA - TTB) / (TRSA - TRSB), \quad (1)$$

where

ΔT = differential travelttime,
TTA= travelttime of transmitter A,
TTB= travelttime of transmitter B,
TRSA=transmitter-receiver spacing A, and
TRSB=transmitter-receiver spacing B.

The pitfall of this method is that all errors in transit-time detection result in large velocity errors and only small sections of the record, therefore, contain useful velocity information. Our method is less elegant than Schlumberger's default computation, which uses four transit times per ΔT ; however, by relying on only two transit times simultaneously, we greatly improved our chance of obtaining valid slowness/velocity data. In order to discern these valuable velocity data, we compared results of one processing technique using data from the two different logging passes or compared the results of the same pass achieved with different techniques.

Two of the total of 13 incorporated data categories and processing techniques described below are subject to human judgement and experience. Some of the data categories use information twice—all of those instances are noted.

Logging Velocity Data Categories

In this section we briefly introduce and discuss the different data categories. To make the chosen abbreviation for the data categories more transparent, two examples are given. The data category "AFA2/1(LTT1 + 2) match av" is composed of "AFA," for analog first arrival, "2/1" comparing pass one and two of transmitter receiver spacing "LTT1" and "LTT2." The additional abbreviation "match av" indicates that matching velocity values of both passes of the same depth have been used to calculate a mean or average value (av) representative for this data category and depth. Data category "2DC2a/DC2 match av" for example is based on velocity values obtained by digital coherency mapping (DC) of wavelets collected during run 2. The abbreviation "a" indicates special processing parameters, explained in detail in the section of the "DC2a/DC2 match av" data category. The abbreviation "match av" again indicates that matching velocity values of both processing types (DC2a and DC2) of the same depth have been used to calculate a mean value representative for this data category and depth.

AFA2/1(LTT1 + 2) Match Av

This category uses transit times LTT1 (10-ft spacing) and LTT2 (8-ft spacing). Calculated velocities of the first and second passes are compared. Using a 300 m/s quality criteria, all data that exceed this velocity difference are excluded from passes one and two. Data within this range are included using an average velocity of the first and second passes. Long-spaced transmitter and receiver pairs may be favorable in lithologic units with strong velocity inhomogeneities within the depth resolution of the tool because they integrate over a larger rock volume.

AFA1(LTT1 + 2) and AFA2(LTT1 + 2) Picked by Log Character

This graphical method uses the two transit-time plots of the two receiver/transmitter pairs LTT1 and LTT2 and the resulting velocity plot

of each pass without comparing the two passes with each other and without looking at absolute velocity values. We believe that the DT calculated from these two transit times merits special attention; of all the transit times recorded, LTT1 and LTT2 performed best. This is based on the subjective experience of the logging engineer, observation of the waveforms during acquisition, and log quality control standards set forth by Schlumberger (Bateman, 1985). Admitting that this method is largely subjective, it is nevertheless an independent approach to extract useful data. The major advantage of this method compared to the previous category (AFA2/1[LTT1 + 2] match av) is that it is entirely focused on repeatability. Tool position, noise level, and a number of other variables can cause differences in quality and lack of repeatability between passes. In this category, valuable information from one pass that has no counterpart in the other pass can be included.

AFA1(LTT1, -2, -3, -4; TT1, -2, -3, -4) and AFA1(LTT1, -2, -3, -4; TT1, -2, -3, -4) High, and AFA2(LTT1, -2, -3, -4) and AFA2(LTT1, -2, -3, -4) High

These data categories are the result of an unusual statistic and combinatorial processing approach. We computed differential transit times for all available transmitter and receiver spacings (LTT1, -2, -3, and -4; and TT1, -2, -3, and -4). For N number of initial transit times it is possible to generate q number of combinations:

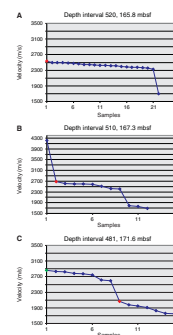
$$q = \frac{1}{2} (N^2 - N). \tag{2}$$

Using all recorded transit times with their respective geometries, besides the six values of the wideband receiver array (Fig. F4), there are 28 possible and 26 actual resulting velocities for the first pass, as two transmitter/receiver pairs have the same spacing (LTT1/LTT4 and TT1/TT4). Unfortunately, TT1, -2, -3, and -4 transit times were not recorded for the second logging pass. Consequently, only five velocity combinations are possible. The resulting velocities for each pass were then compared (Eq. 2), leading to 325 combinations for the first pass and 10 combinations for the second pass. The confidence level was again ≤ 300 m/s difference in velocity. Additionally, all average resulting velocities < 1500 m/s (water velocity) and > 6000 m/s have been excluded.

For logging pass two, with 10 possible average velocities for each depth interval, the values were mostly within a narrow range and a simple average was calculated as a result for this pass and category. In the case of two distinct populations, the higher value in the AFA2(LTT1, -2, -3, -4) high category was saved. Only 159 out of 1050 possible values in the depth interval 85–243 mbsf met the criteria.

For logging pass one, with 325 possible average velocities for each depth interval, up to 117 actual values were received using the 300 m/s confidence interval and the plausibility range of 1500–6000 m/s. As a guide for decision making, the values of the first pass were sorted in descending order, and small graphs were plotted for most of the depth intervals (Fig. F5). Four cases are common. Typically, the values have a stable plateau at the high-velocity side (Fig. F5A) and only some anomalies at the low side of the values. The choice of high velocities for a final value for this depth interval and category is based on the observation that analog picking in noisy, highly attenuated signals of our log commonly resulted in velocities lower than those expected. Additionally, all signals that travel only through drill slurry will produce

F5. Data categories for depth intervals, p. 21.



lower velocities. However, at several depth intervals, erratic velocities were also observed at the high end of the velocity spectrum (Fig. F5B). These values may be the result of cable noise, malfunctioning transducers, or waves traveling alongside the tool. In both cases (Fig. F5A, F5B), the erratic values are relatively easy to detect. Their numbers are commonly small compared to the population of reasonable values, and usually the erratic values differ significantly from the majority of the values for the same depth interval and values of preceding and subsequent depth intervals. Since the aperture of measurement with this technique (equal to the distance between the two receivers used) is between 2 and 9 ft, abrupt changes in measured velocity from one 6-in depth interval to another are unlikely, even if the geological profile contains sudden major impedance changes. During the semiautomatic sorting and evaluation of the values, depth intervals with two distinct bimodal velocity populations were also evident (Fig. F5C). Because decisions are likely to be biased in those instances, the higher values were included in a separate category (AFA1[LTT1, -2, -3, -4; TT1, -2, -3, -4] high), similar to the high values of the second logging pass. A total of 751 out of 793 possible values in the depth interval 124–244 m meet the criteria for category AFA1(LTT1, -2, -3, -4; TT1, -2, -3, -4). Nonconclusive velocities were found for 5% of the depth intervals for this category and pass.

AFA1/2(LTT1, -2, -3, -4; TT1, -2, -3, -4) Match Av

This category compares values of the previous categories AFA1(LTT1, -2, -3, -4; TT1, -2, -3, -4) and AFA2(LTT1, -2, -3, -4). The average of velocity values of the same depth interval with a difference of ≤ 300 m/s between the first and second pass were incorporated. Although this category introduces data twice into the initial data pool without utilizing new processing aspects, it seemed especially important to emphasize agreeing results of the first and second pass. More than 80% of the few values (112) in the depth interval 124–243 mbsf found in pass one (category AFA2[LTT1, -2, -3, -4]) matched their depth counterparts in logging pass two (category AFA1[LTT1, -2, -3, -4; TT1, -2, -3, -4]).

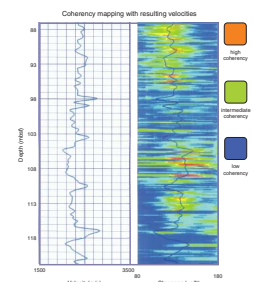
DC1/2 Match Av

Digital coherency mapping output is based on the eight digitized wavelets received at the wideband receiver array (Fig. F4) as described above. In depth intervals with low coherency and disturbed signals, the coherency mapping technique has a tendency to produce significantly higher velocities than the velocities derived by analog picking. The category DC1/2 match av contains average velocity values of the first and second pass (see Fig. F6 for an example of data of the second logging run) calculated from values with a difference of 300 m/s or less for a specific depth interval. Of the 783 velocities acquired in both logging runs for the same depth intervals, 518 meet the 300 m/s criteria (66%).

DC2 High Coherency

This category represents velocity values derived by coherency mapping of the recorded wideband receiver array of the second logging pass. Only depth intervals with excellent coherency values, indicating stable receiver signals, were included. This category may contain information that has already been used within the previous category. Nevertheless, it is important to regard additional valuable data which is only

F6. Digital coherency mapping with resulting velocities, p. 23.



tion for 60% of the core. In order to produce a continuous velocity log for subsequent users, the following assumptions were made based on the available data. Considering the laboratory velocity and density data (Shipboard Scientific Party, 1999b), low-recovery zones are commonly located at acoustic impedance changes. We, therefore, assume that all major impedance changes are represented within the available data. Furthermore, in order to reduce data gaps by two-thirds of their depth interval, we added artificial data points at both ends of the gap. This measure is supported by the observation of discrete changes in sedimentology within the cores recovered (interchange of clast rich structureless diamictite with more sorted sands and silts). Using a simple interpolation technique to fill the data gaps would have caused unrealistic continuous transitions within the velocity profile that are also nonpreferable for later seismic modeling (e.g. synthetic seismograms).

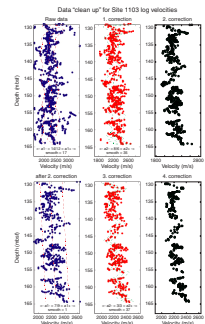
RESULTS AND DISCUSSION

All the data derived from the previously described 13 processing techniques categories (without the laboratory-derived velocities) incorporated into the initial data pool from 0 to 244 mbsf are shown in Figure F7. The data are also given in Table T2. We merged all data categories with a total of 5400 values into a single depth/velocity matrix by offsetting the depth of the individual velocity categories by 5 mm. Looking at the hole section in a compressed representation, it is difficult to detect well-supported trends (Fig. F7). Although only data that passed several quality criteria were included, the data set remains extremely spiky and velocity variations of 1600 to 2800 m/s for the same depth interval are common. Based on the large standard deviation of the data, we rejected a simple smoothing of the values. Our first step toward simplifying the data were carried out in 25-m sections. We used our own method as described in the “Seismic Stratigraphy” section of the “Explanatory Notes” chapter of the Leg 178 *Initial Reports* volume (Shipboard Scientific Party, 1999a). This method is based on individual polynomial fittings of variable orders and uses selectable confidence intervals around the polynomial fit. An example of a six-step cleanup is given in Figure F8. An interpolated trendline connecting values chosen is shown together with the initial data pool in Figure F7 (blue line). It should be noted that the polynomial fitting and exclusion technique will always favor incorporating regions with high data density. In most cases, this is an improvement over simple averaging, since outliers are completely removed and do not affect the resulting data. On the other hand, this method by no means ensures the extraction of only good data out of clusters in case the majority of the data for one depth interval is erroneous and the described data separation technique fails.

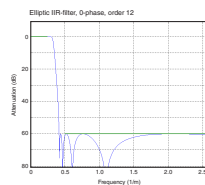
Subsequently, the data were filtered with a low-pass filter (Fig. F9) designed to filter out short wavelength variations. The frequency range of the pass band is set to reduce the vertical resolution of the filtered velocity log to approximately 2 m. The final representation of our approach is given in Figure F10. All data processing within this study is based on raw unsynchronized data with respect to depth shifts between logging runs and with respect to the different transmitter receiver pairs used for the different data categories. To achieve a comparable profile with regard to other depth-shifted logging data processed by the Lamont-Doherty Earth Observatory Borehole Research Group (LDEO-BRG), the resulting data were graphically fitted with the integrated re-

T2. Velocity categories, p. 32.

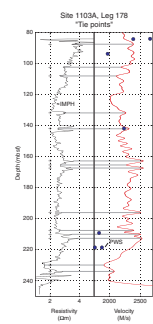
F8. Example of data reduction, p. 25.



F9. Plot of a low-pass filter that removes short-wavelength variations, p. 26.



F10. Reduced and filtered logging velocity data synchronized with depth-shifted resistivity data, p. 27.



sistivity (IMPH) data. The program used is AnalySeries 1.2 (Paillard et al., 1996), and the 14 matchpoints and resulting depth shifts are given in Table T3 and Figure F10. According to the LDEO-BRG depth scale, the resulting depth shifts are larger near the drill pipe between 87 and 100 mbsf, very reasonable in the interval 100 to 207 mbsf and 230–244 mbsf, and unrealistic high in the short interval between 207 and 212 mbsf. The higher shift values at the base of the drill pipe may be due to problems encountered during the process of reentering the tools after the logging run (Shipboard Scientific Party, 1999b). Variable shift values between 0 and 3 m can be easily explained with a combination of three effects:

1. During the data processing at LDEO-BRG, the GHMT log was used as the reference for depth-matching. The maximum depth shift of the TC (including the resistivity log) relative to the reference log was between 1 and 2 m. The maximum shift applied to the two FMS-sonic logging runs was an additional 0.6 m.
2. The maximum receiver transmitter spacing on the sonic tool is 13.5 ft (~4.1 m). During the data processing, the traveltime information of different transmitter receiver pairs with different spacings and effective integrative depth range was brought together without calibrating the sensor-pairs to their effective depth and without synchronizing the two logging runs individually beforehand.
3. The low-pass filtering of the data was accompanied by a reduction of the depth resolution to 2 m.

In the final velocity profile, the effect of those three factors is combined to various degrees depending on the varying importance of a single data category for a specific depth interval to the finally chosen data. However, the large shifts in the depth interval 207–212 mbsf are probably unrealistic and the result of a mismatch or incorporation of erratic data into the final velocity data selection. Since the correlation is entirely based on graphical correlation with the same systematics for the whole section (matching regional highs and lows of the reference with regional highs and lows of the filtered data curve), and given that the erroneous interval is very short, we decided to stick to the correlation and accepted its limitations in the mentioned depth interval 207–212 mbsf.

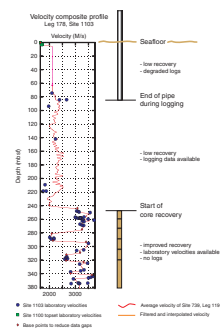
Finally, after compiling the data from all depth sections (0–75, 75–244, and 244–360 mbsf), the contacts were smoothed, resulting in a continuous profile that is displayed together with the laboratory velocity data values (Fig. F11, Table T4).

The computed velocity curve can be compared for validation to the other representative downhole logs obtained at Site 1103 (Shipboard Scientific Party, 1999b): the neutron porosity (APLC), the bulk density (RHOM), the electrical self-focusing resistivity (SFLU), and the magnetic susceptibility (RMGS) (Fig. F12). The chosen logs show reliable values, except the anomalous ones in the RMGS log (~117 mbsf), certainly caused by the APS bow spring lost in the hole.

The velocity curve is general correlated with the RHOM, RMGS, and SFLU logs, and anticorrelated with the APLC log. The velocity curve shows the same features as the other logs that are divided in five units (Fig. F12). The first unit is characterized by low porosity and high resistivity, density, and velocity values. The second unit exhibits porosity values between 25% and 50% and lower susceptibility, density, velocity, and resistivity values. It is interesting to point out that the thin beds

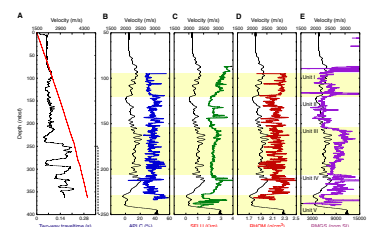
T3. Absolute depth shifts, Site 1103, p. 33.

F11. Composite velocity profile, Site 1103, p. 28.



T4. Final depth vs. velocity and depth two-way travelttime data, p. 34.

F12. Velocity comparisons, p. 29.



(~132 and ~142 mbsf) seen in all the logs (high SFLU and RHOM values; low NPHI and RMGS values) are also found in the velocity curve. In the third unit, the resistivity, the susceptibility, and the velocity logs show the same higher values at the top with a slight tendency to decrease down the hole. The fourth unit is characterized by a sharp reduction of the previous logs and a sharp increase in the porosity values. In the last unit, we note a distinct jump to lower density, resistivity, susceptibility, and velocity values and higher porosity. The high variability of the logs in this part is not seen in the velocity curve, probably because of the smoothing method used to reconstruct it.

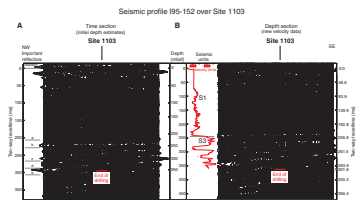
Additionally we present a comparison of the original seismic data and a depth-migrated section generated by using the new velocity data. The original time section already published in the Leg 178 *Initial Reports* volume (Shipboard Scientific Party, 1999b), the new velocity data, and the migrated depth section are shown in Fig. F13. The data presented confirm the location of the major shelf unconformity at 222 ms TWT, or 243 mbsf. The unconformity between seismostratigraphic units S1 and S3 (Shipboard Scientific Party, 1999b) is seismically expressed by a strong negative and subsequent positive reflection around 222 ms TWT below seafloor (Fig. F13A). The decline and rise in acoustic impedance (acoustic impedance = velocity \times density) within the depth interval 220 to 245 mbsf seen in the velocity and density data of Figure F12D are most likely the cause of this reflector. The positive reflection around 206 ms TWT on the other hand, is probably still part of the S1 topset package.

CONCLUSIONS

Starting with nonconclusive velocity logs as a result of difficult-to-log slow formation with extremely high internal velocity contrasts and the harshness of an uncentered logging tool string due to the need to log without the centralizing bow springs, we tried to improve the quality of the data obtained and present measures to evaluated data previously inaccessible with standard processing techniques. Even though the velocity profile produced correlates well with other logs obtained (neutron porosity, bulk density, self-focusing electrical resistivity data, and magnetic susceptibility) (Fig. F12) and offers a reasonable estimate for the location of a prominent shelf unconformity, we should emphasize the limitations of the data. Possible errors introduced may result from

1. A bias in choosing and defining the data categories;
2. The possibility of exclusion of rare good data in a given interval where misleading values represent the majority of the data;
3. An uncertainty of the precise depth location of data from transmitter and receiver spacings that are collecting different regions along the tool string for a given tool position;
4. The mixing of non-depth shifted raw data of logging runs one and two; and
5. A bias in the final correlation and no linear depth shift to the resistivity log using the only general guideline that low resistivity zones are most commonly denser and, therefore, acoustically faster.

F13. Comparisons of time and depth section of line I95-152 in the vicinity of Site 1103, p. 30.



Nevertheless, in contrast to seismically derived velocity information (Tinivella et al., [Chap. 16](#), this volume) the velocity information presented here is still more detailed and allows the investigation of the seismic character at least on the scale of the defined logging units (Fig. [F12](#)). We hope that the new data will help seismostratigraphers, modelers, and sedimentologists to uncover the beauties and complexities of the Antarctic shelf.

ACKNOWLEDGMENTS

We thank the Ocean Drilling Program, crew members, technical staff, the captain of the *JOIDES Resolution*, the co-chiefs, and other scientists who made this venture possible. Thanks to our spouses and children for letting us go and for spending their time to improve this paper. Special thanks to Christian Bucker and Trevor Williams for their constructive insight in final reviewing and improving this manuscript. We also thank Dr. Warner Brückmann, Daniel A. Hepp, Jayne Welling-Wolf, and Ortrud Runze for early reviews, linguistical help and technical support in preparing this report. This research used samples and/or data provided by the Ocean Drilling Program (ODP). ODP is sponsored by the U.S. National Science Foundation (NSF) and participating countries under management of Joint Oceanographic Institutions (JOI), Inc. This research was supported by “SPP DSDP/ODP” Grant TH 200/37-1 and 2 of Deutsche Forschungsgemeinschaft.

REFERENCES

- Barker, P.F., Barrett, P.J., Camerlenghi, A., Cooper, A.K., Davey, F.J., Domack, E.W., Escutia, C., Kristoffersen, Y., and O'Brien, P.E., 1998. Ice sheet history from Antarctic continental margin sediments: the ANTOSTRAT approach. *Terra Antarct.*, 5:737–760.
- Bateman, R.M., 1985. *Log Quality Control*: Boston (Int. Human Resour. Dev. Corp. Press).
- Camerlenghi, A., Rebesco, M., DeSantis, L., Volpi, V., DeRossi, A., in press. The Antarctic Peninsula Pacific Margin: modelling flexure and decompaction with constraints from ODP Leg 178 initial results. In Gamble, J., Skinner, D., and Henrys, S. (Eds.), *Proc. 8th Int. Symp. Antarct. Earth Sci., N. Z. J. Geol. Geophys.*: Wellington (Royal Society of New Zealand).
- Dresen, L., 1985. Flözwellenseismik für die untertägige Steinkohlenerkundung. In Bender, F. (Ed.), *Angewandte Geowissenschaften (Vol. 2): Methoden der Angewandten Geophysik und mathematische Verfahren in den Geowissenschaften*: Stuttgart (Ferdinand Enke Verl.), 261–293.
- Eyles, N., Daniels, J., Osterman, L.E., and Januszczak, N., 2001. Ocean Drilling Program Leg 178 (Antarctic Peninsula): sedimentology of glacially-influenced continental margin topsets and foresets. *Mar. Geol.*, 178:135–156.
- Hambrey, M.J., Ehrmann, W.U., and Larsen, B., 1991. Cenozoic glacial record of the Prydz Bay continental shelf, East Antarctica. In Barron, J., Larsen, B., et al., *Proc. ODP, Sci. Results*, 119: College Station, TX (Ocean Drilling Program), 77–132.
- Larter, R.D., and Barker, P.F., 1989. Seismic stratigraphy of the Antarctic Peninsula Pacific margin: a record of Pliocene-Pleistocene ice volume and paleoclimate. *Geology*, 17:731–734.
- , 1991. Effects of ridge-crest trench interaction on Antarctic-Phoenix spreading: forces on a young subducting plate. *J. Geophys. Res.*, 96:19583–19607.
- Larter, R.D., Rebesco, M., Vanneste, L.E., Gamboa, L.A.P., and Barker, P.F., 1994. Seismic reflection investigations on the Pacific margin of the Antarctic Peninsula. In Cooper, A.K., Barker, P.F., and Brancolini, G. (Eds.), *Geology and Seismic Stratigraphy of the Antarctic Margin*. Antarct. Res. Ser., 68:271–274.
- , 1997. Cenozoic tectonic, sedimentary and glacial history of the continental shelf west of Graham Land, Antarctic Peninsula. In Cooper, A.K., Barker, P.F., and Brancolini, G. (Eds.), *Geology and Seismic Stratigraphy of the Antarctic Margin (Pt. 2)*. Antarct. Res. Ser., 71:1–27.
- Paillard, D., Labeyrie, L., and Yiou, P., 1996. Macintosh program performs time-series analysis. *Eos*, 77:379.
- Rebesco, M., Camerlenghi, A., and Zanolla, C., 1998. Bathymetry and morphogenesis of the continental margin west of the Antarctic Peninsula. *Terra Antarct.*, 5:715–728.
- Schlumberger, 1989, *Log Interpretation Principles/Applications*: Houston (Schlumberger Educ. Services), SMP-7017.
- Shipboard Scientific Party, 1989. Site 739. In Barron, J., Larsen, B., et al., *Proc. ODP, Init. Repts.*, 119: College Station, TX (Ocean Drilling Program), 289–344.
- , 1999a. Explanatory notes. In Barker, P.F., Camerlenghi, A., Acton, G.D., et al., *Proc. ODP, Init. Repts.*, 178, 1–66 [CD-ROM]. Available from: Ocean Drilling Program, Texas A&M University, College Station, TX 77845-9547, U.S.A.
- , 1999b. Shelf Transect (Sites 1100, 1102, and 1103). In Barker, P.F., Camerlenghi, A., Acton, G.D., et al., *Proc. ODP, Init. Repts.*, 178: College Station, TX (Ocean Drilling Program), 1–58.
- , 1999c. Leg 178 summary: Antarctic glacial history and sea-level change. In Barker, P.F., Camerlenghi, A., Acton, G.D., et al., *Proc. ODP, Init. Repts.*, 178: College Station TX (Ocean Drilling Program), 1–58.

Ten Brink, U.S., and Cooper, A.K., 1992, Modeling the bathymetry of Antarctic continental margins. *In* Yoshida, Y., Kaminuma, K., and Shiraishi, K. (Eds.), *Recent Progress in Antarctic Earth Science*: Tokyo (Terra Publ.), 763–772.

Figure F1. Northwest-southeast air gun multichannel seismic reflection profile showing the locations of sites drilled along a shelf transect during ODP Leg 178 (Shipboard Scientific Party, 1999c). Hole 1103A recovered/penetrated sediments of the topsets (Unit S1) and foresets (Unit S3). Average recovery at Site 1103 is 12.3% and only 2.6% for Unit S1. Note also the low recoveries at the other sites along the transect. The bathymetric map of the continental margin west of the Antarctic Peninsula (Rebesco et al., 1998) indicates the location of the shelf transect sites and the approximate location of seismic line I95-152 (white line). ([Figure shown on next page.](#))

Figure F1 (continued). (Caption shown on previous page.)

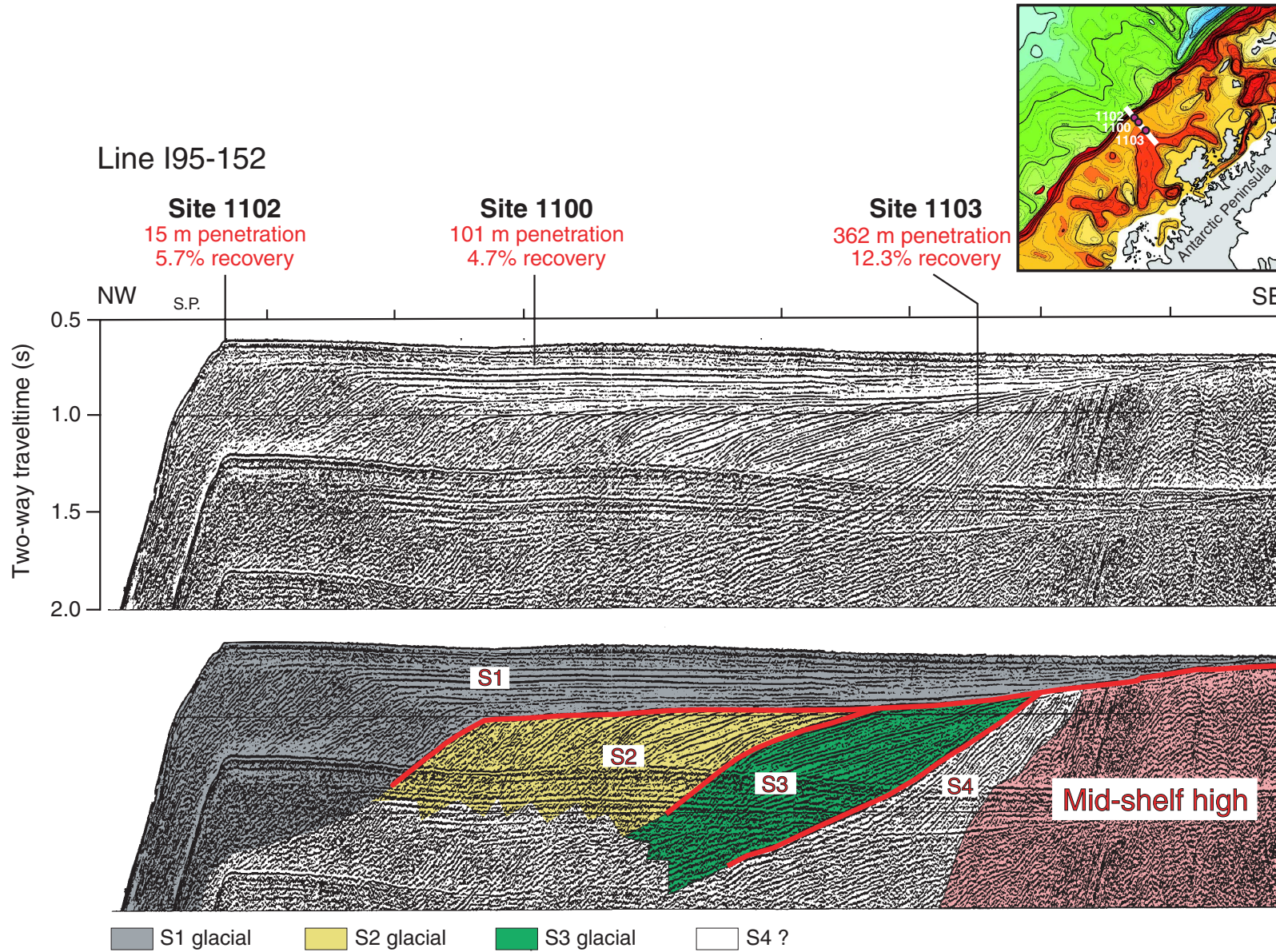


Figure F2. Compiled ODP/DSDP velocity data from topset environments in the Prydz Bay and Ross Sea continental shelves. We used an average velocity calculated from logging data from Site 739 of Leg 119 (Shipboard Scientific Party, 1989).

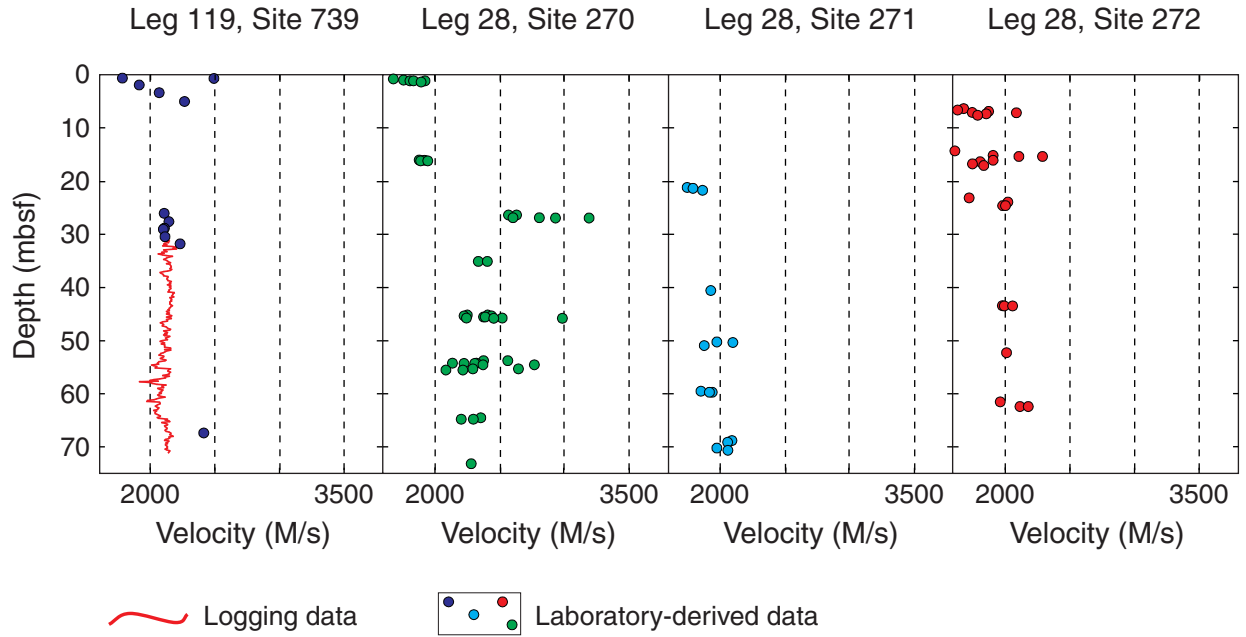


Figure F3. Schematic drawing of the FMS-sonic tool string used at Site 1103 of Leg 178. Note that the MCD centralizer unit that normally is part of the assembly was not deployed at this site.

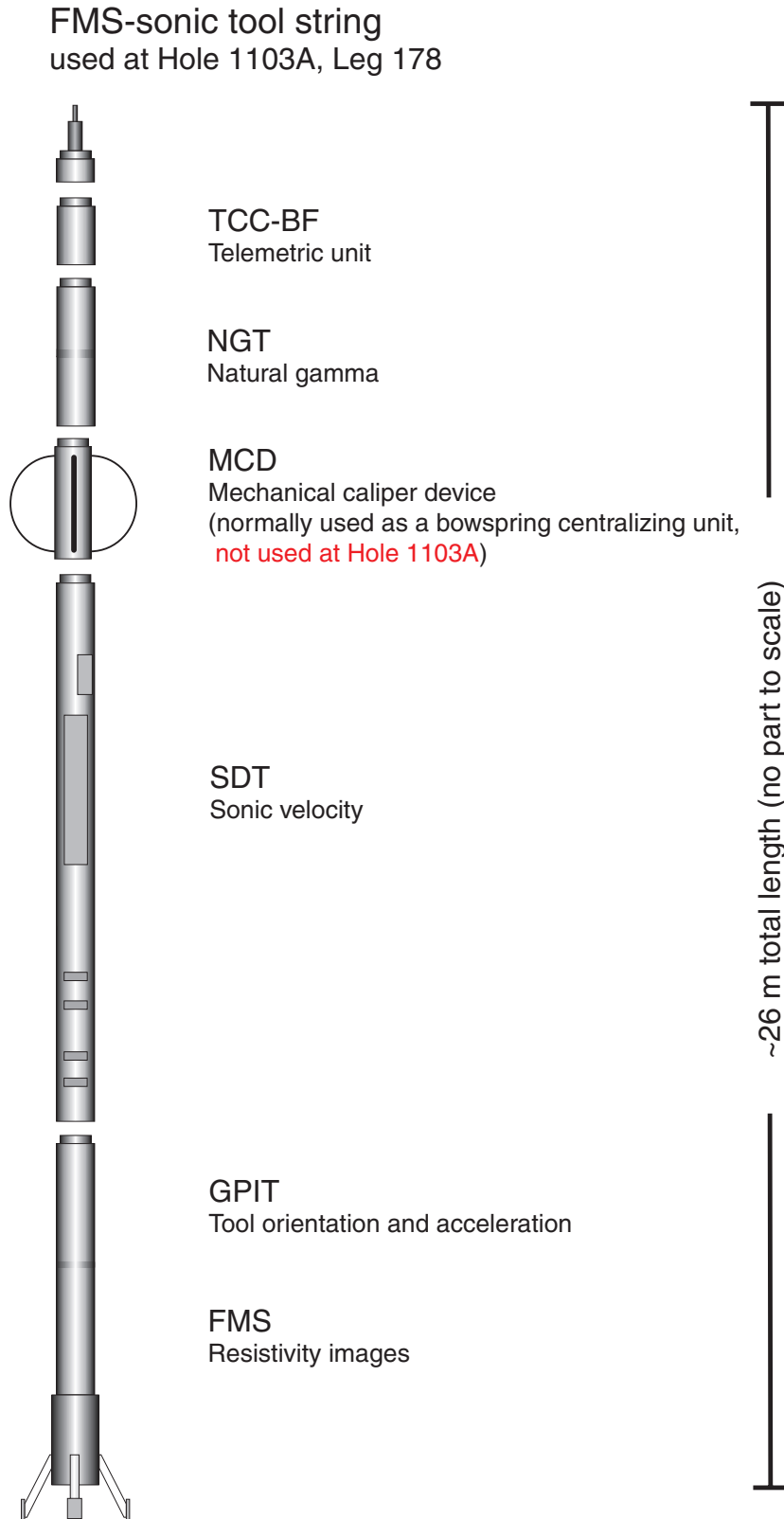


Figure F4. Detailed drawing of the transmitter and receiver configuration of the SDT sonic velocity tool. The “mud” transmitter and receiver near the top of the tool were not used.

SDT sonic velocity

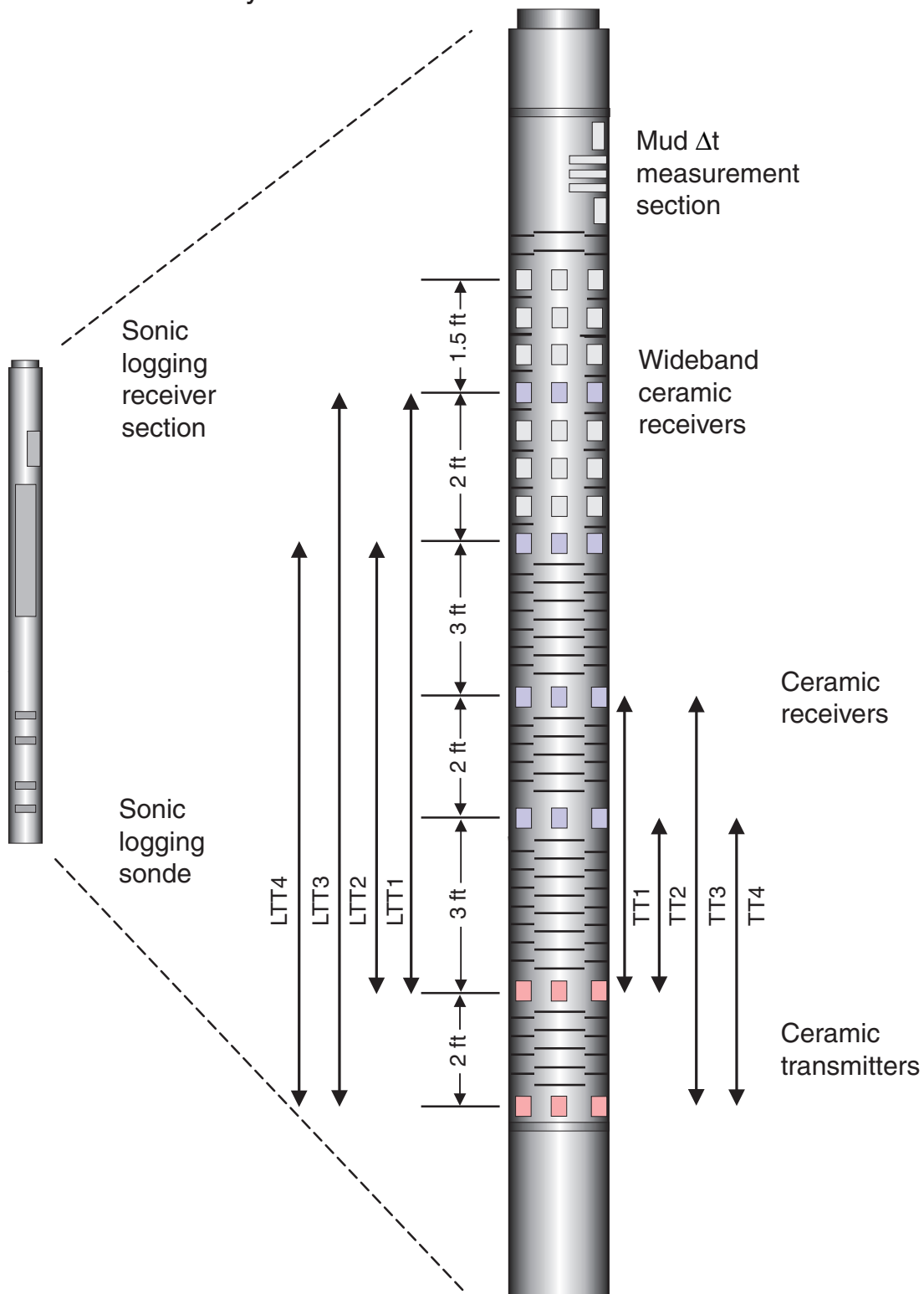


Figure F5. The data categories AFA1(LTT1, -2, -3, -4; TT1, -2, -3, -4) high, as well as AFA2(LTT1, -2, -3, -4) and AFA2(LTT1, -2, -3, -4) high, are the result of a statistical and combinatorial processing approach. We calculated differential transit times for all available transmitter and receiver spacings (LTT1, -2, -3, -4 and TT1, -2, -3, -4) based on analog picked first arrivals. As a guide for decision making, all resulting velocity combinations were sorted in descending order and plotted into small graphs for most of the depth intervals. Four cases are common. **A.** Typically, the values have a stable plateau at the high-velocity side and only some anomalies at the low side of the values. **B.** In several depth intervals, we also observe erratic velocities at the high end of the velocity spectrum. **C.** However, depth intervals with two distinct bimodal velocity populations and depth intervals with no velocities within the plausibility range of 1500-6000 m/s are also observed. ([Figure shown on next page.](#))

Figure F5 (continued). (Caption shown on previous page.)

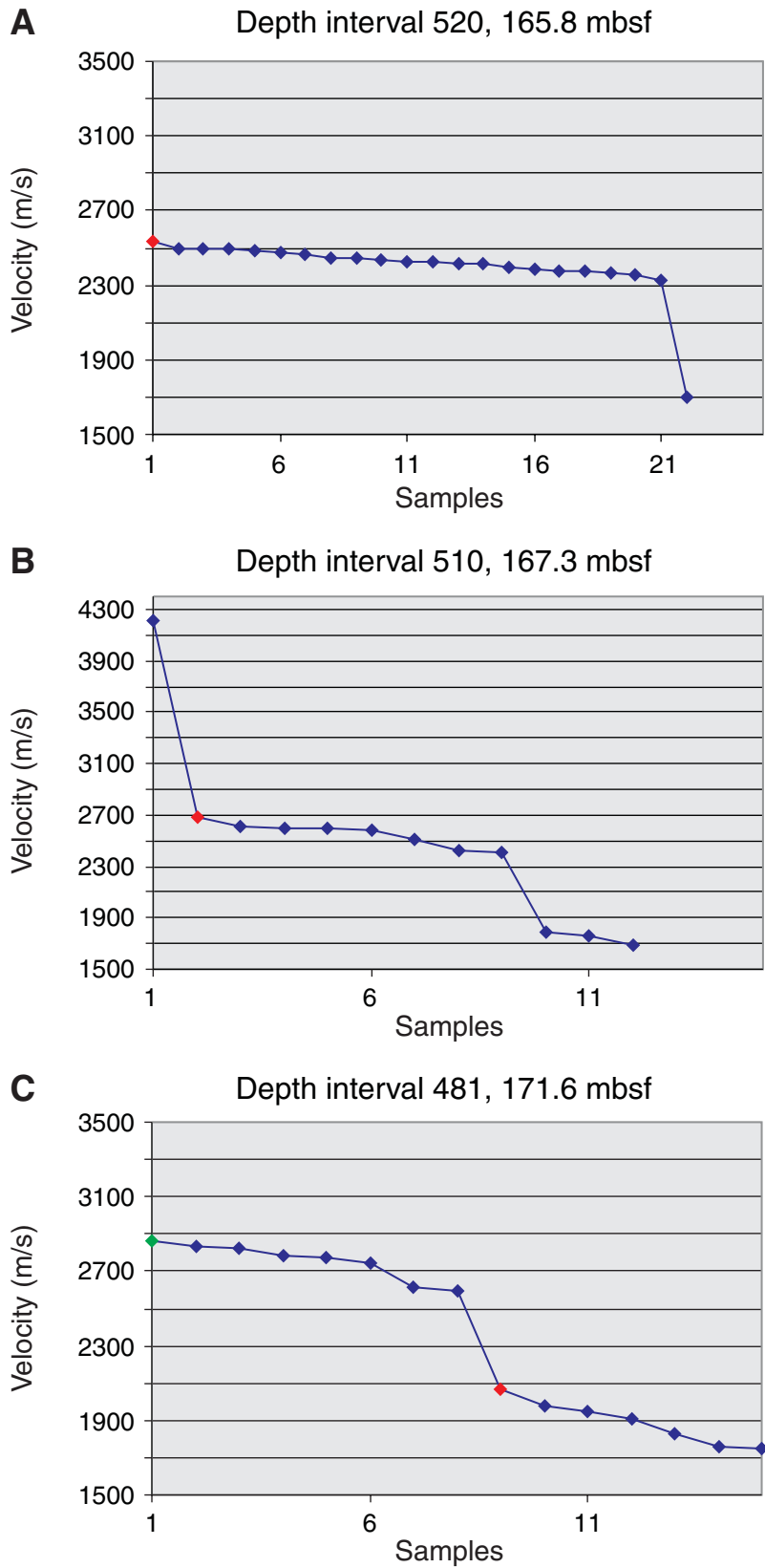


Figure F6. Example of digital coherency mapping performed with data of logging run two. The digital coherency mapping is based on the tracking of highly coherent velocity values. The coherency values within the slowness range (80–180 μs) are color coded (right side of figure). The resulting velocity values are shown on the left side.

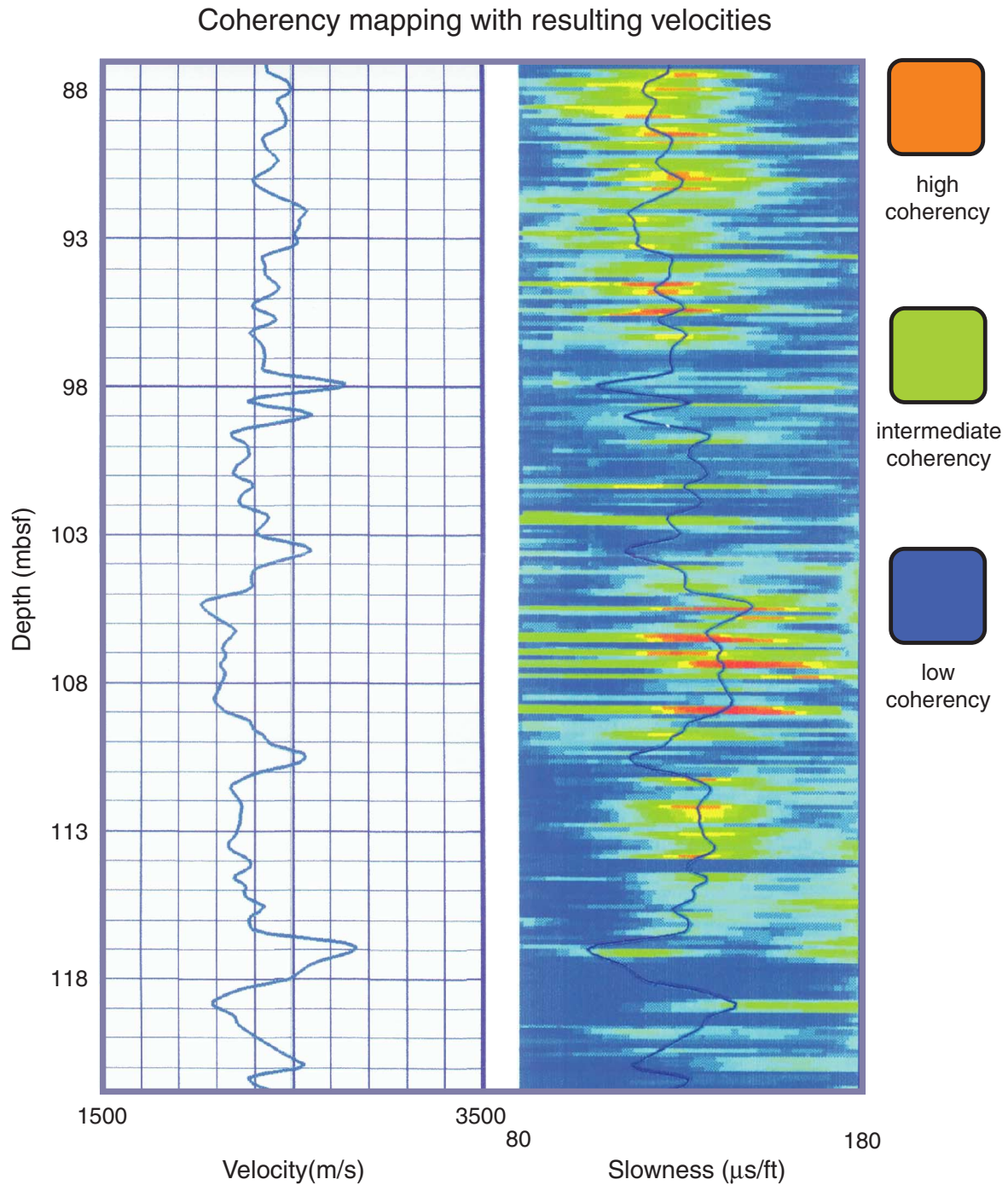


Figure F7. Summary plot of all data categories before data reduction and filtering.

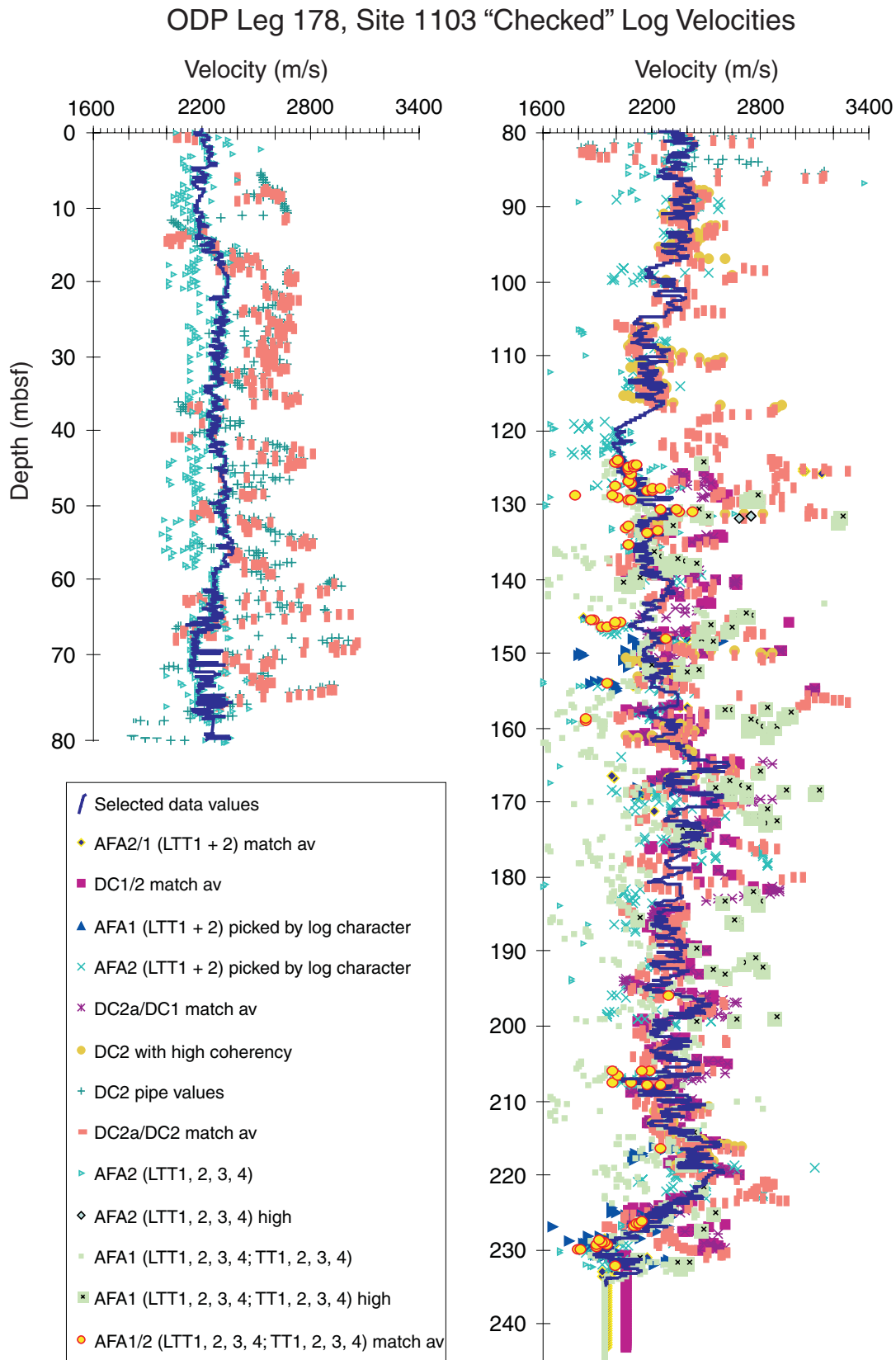


Figure F9. A specially designed low-pass filter is used to remove short-wavelength variations. As a consequence, the depth resolution is reduced to ~2 m.

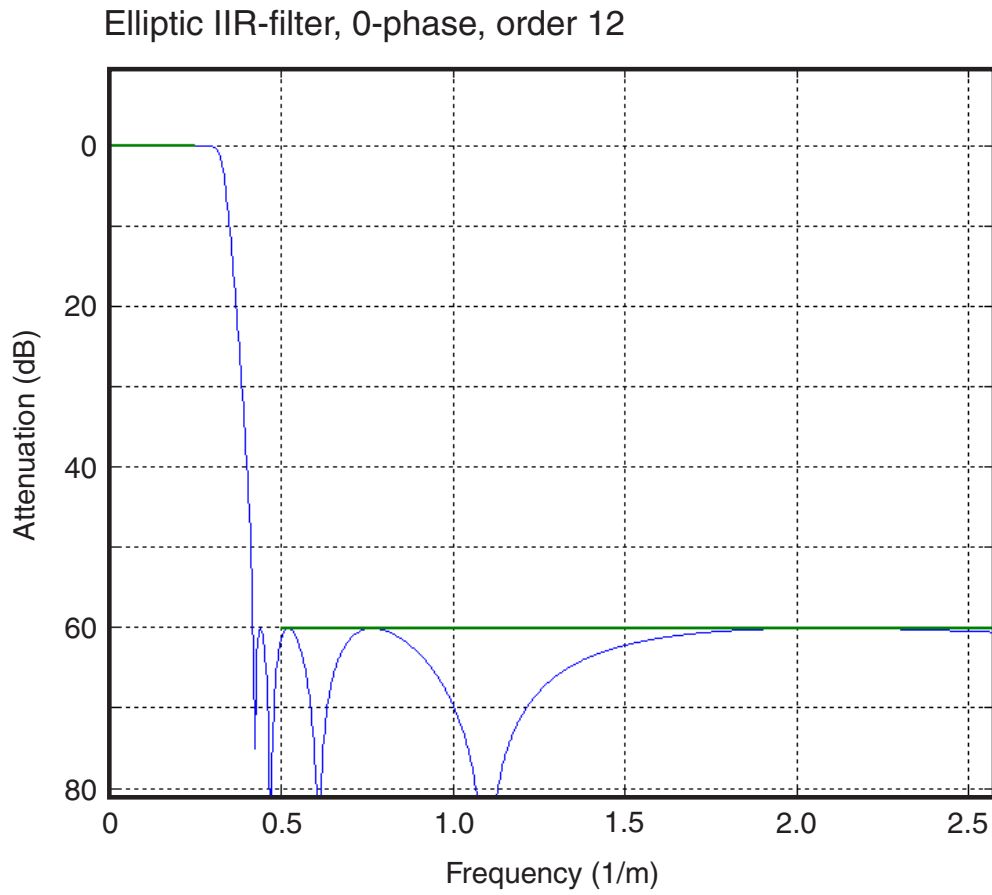


Figure F10. The reduced and filtered logging velocity data are synchronized with the depth-shifted resistivity data (integrated resistivity [IMPH] and self focusing resistivity [SFLU] processed by the Borehole Research Group at Lamont-Doherty Earth Observatory [LDEO-BRG]). Absolute shifts are given in Table T3, p. 33

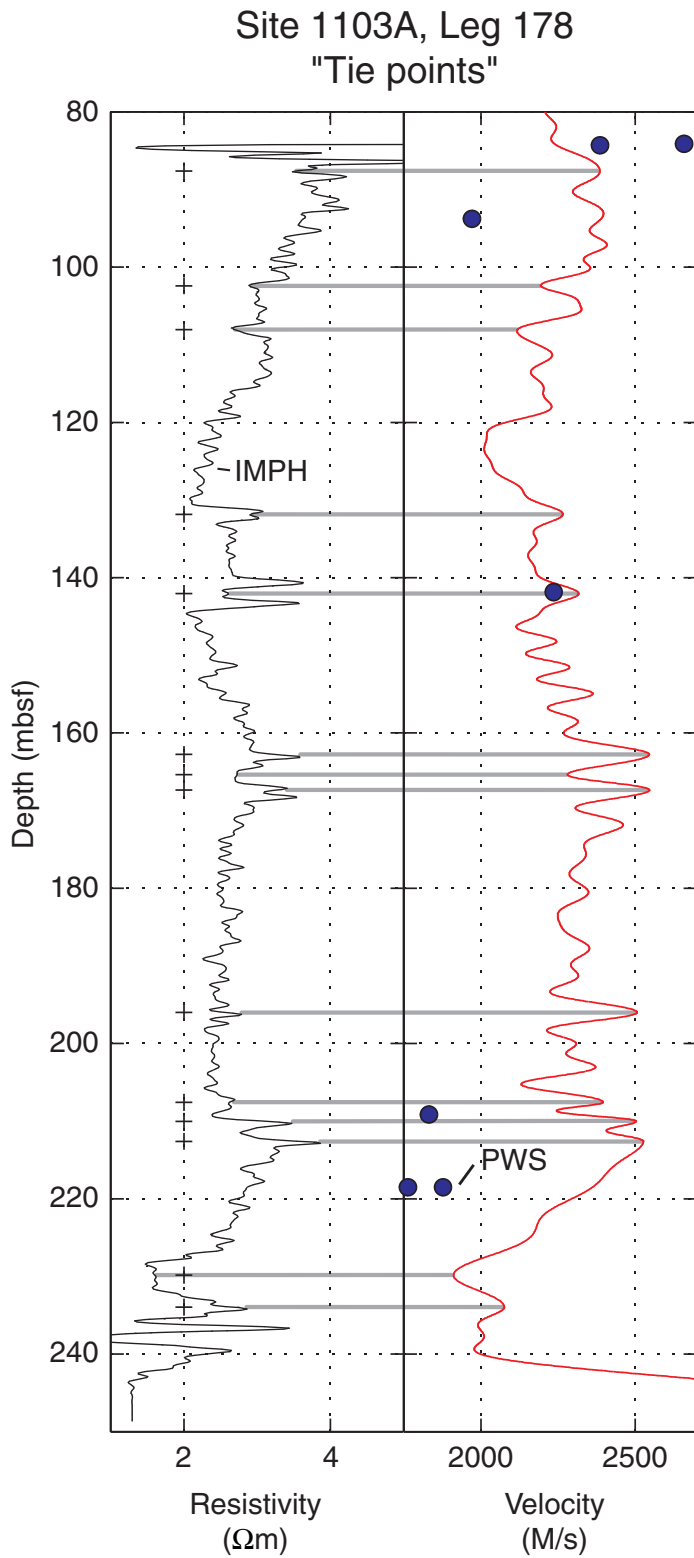


Figure F11. Composite velocity profile of Site 1103 of Leg 178. The different data resources are indicated. A digital version of the composite data can be found in Table T4, p. 34.

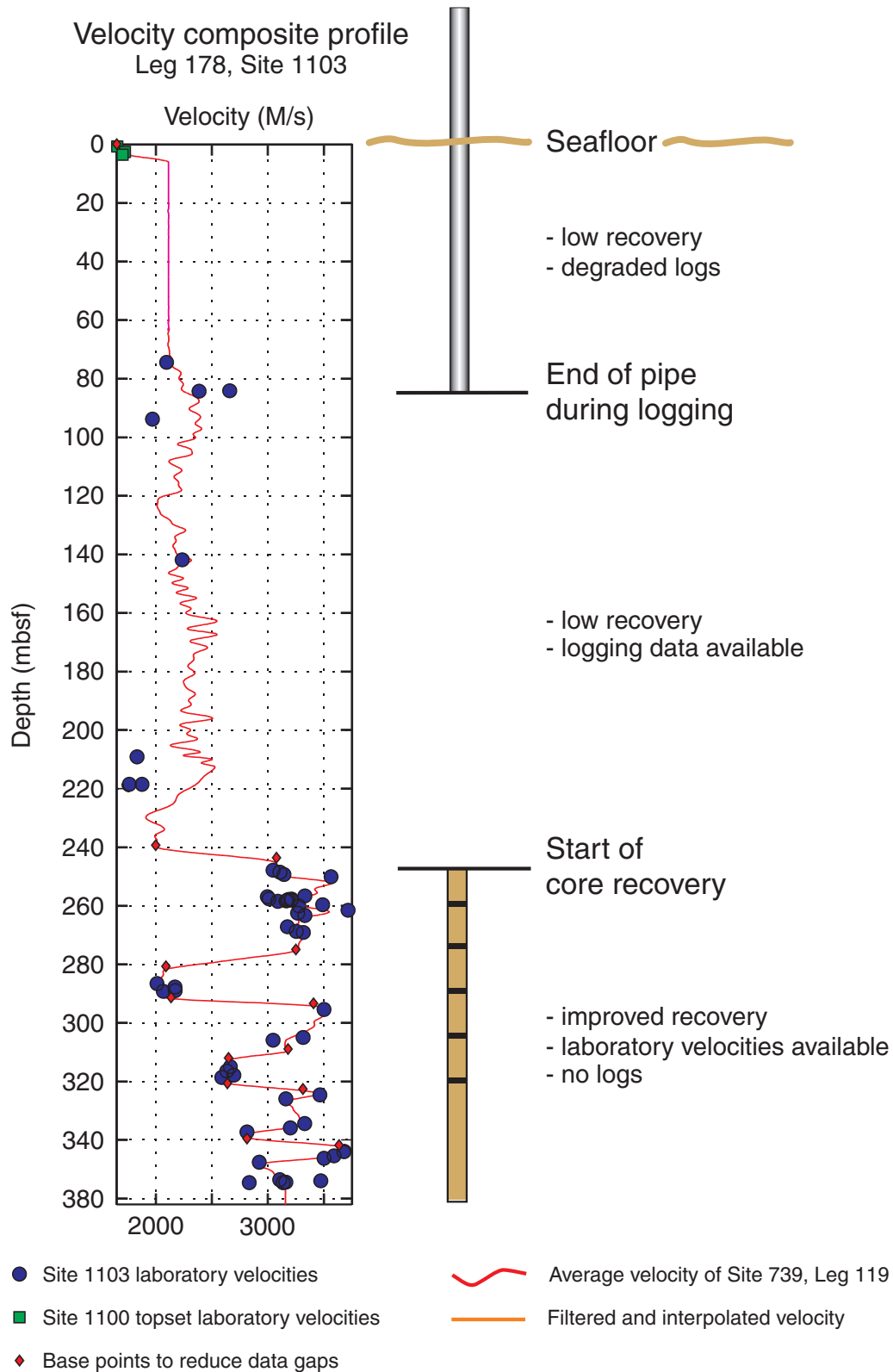


Figure F12. Comparisons of the (A) new velocity data and representative downhole logs, (B) APLC (neutron porosity), (C) SFLU (electrical resistivity), (D) RHOM (bulk density), and (E) RMGS (magnetic susceptibility). The logging units I-V as defined by the Shipboard Scientific Party (1999b) are outlined. Please note the difference in depth for (A) and (B–E).

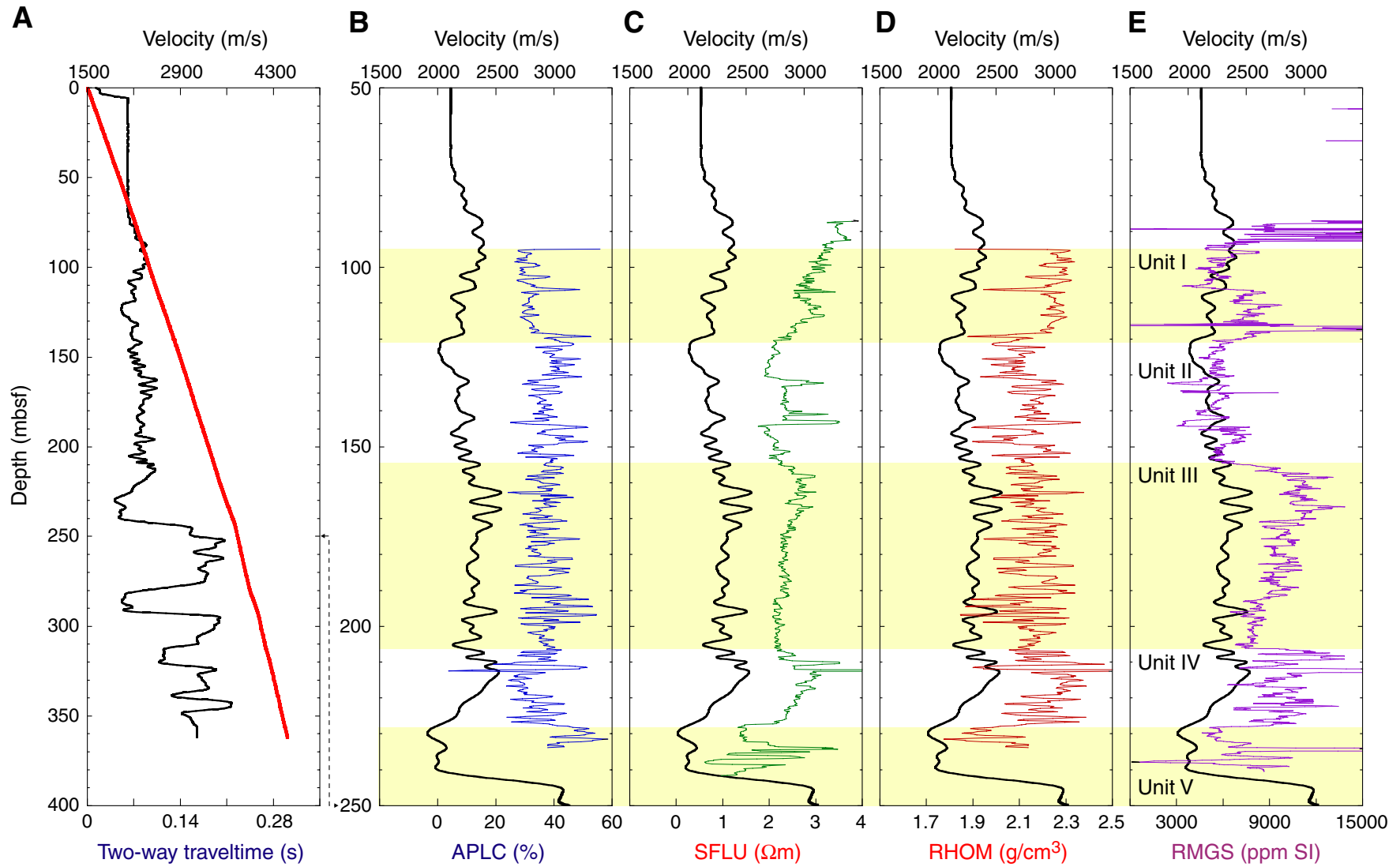


Figure F13. Comparisons of the (A) time and (B) depth sections of line I95-152 in the vicinity of Site 1103. The depth migration is based on the new velocity data. Note the differences in depth scale and apparent S1/S3 geometry between the time section (A) (see figure F36 in Shipboard Scientific Party, 1999b) with an approximate depth annotation, and the depth migrated section presented by this study (B). The presented data confirms the location of the shelf unconformity S1/S3 at 222 ms TWT or 243 mbsf. The unconformity is seismically expressed by a strong negative and subsequent positive reflection. Please refer to Shipboard Scientific Party (1999b) for a detailed description of seismic units and major reflectors (a–e) shown in (A).

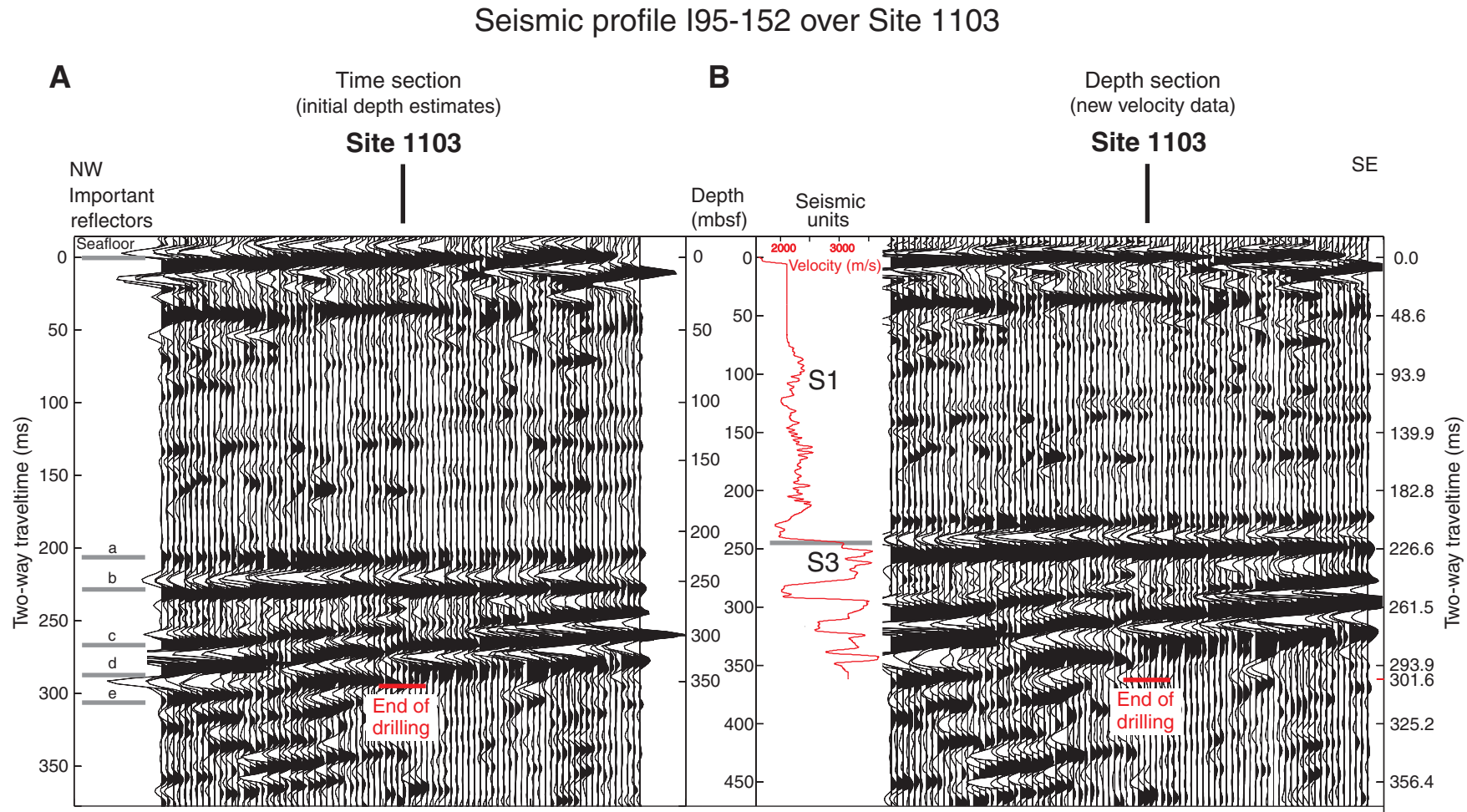


Table T1. Transmitter/receiver spacings of the SDT sonic velocity tool.

Transmitter receiver pair:	TT1	TT2	TT3	TT4	LTT1	LTT2	LTT3	LTT4
Transmitter spacing (ft):	5	3	7	5	10	8	12	10

Notes: Transmitter/receiver spacings of the standard output of the SDT sonic velocity tool without the wideband ceramic receiver array (see Fig. F4, p. 20, for a graphic representation and localization).

Table T2. Data pool of velocity categories used in this study.

Depth (mbsf)	Round depth (mbsf)	Depth + 3.0 cm (mbsf)	AFA(LTT1 + 2) Picked by log character	Depth + 2.5 cm (mbsf)	AFA2(LTT1+2) Picked by log character	Depth + 2.0 cm (mbsf)	AFA2/1(LTT1 + 2) Match av	Depth + 1.5 cm (mbsf)	AFA1(LTT1,-2, -3: TT1, -2, -3, -4)	Depth + 1.0 cm (mbsf)	AFA1(LTT1,-2, -3, -4; TT1, -2, -3, -4) High	Depth + 0.5 cm (mbsf)
244.760	244.760	244.790		244.785		244.780		244.775	1942.725	244.770		244.765
244.608	244.610	244.640		244.635		244.630		244.625	1942.725	244.620		244.615
244.455	244.460	244.490		244.485		244.480		244.475	1942.725	244.470		244.465
244.303	244.300	244.330		244.325		244.320		244.315	1942.725	244.310		244.305
244.150	244.150	244.180		244.175		244.170		244.165	1942.725	244.160		244.155
243.998	244.000	244.030		244.025		244.020		244.015	1942.725	244.010		244.005
243.846	243.850	243.880		243.875		243.870		243.865	1942.725	243.860		243.855
243.693	243.690	243.720		243.715		243.710		243.705	1942.725	243.700		243.695
243.541	243.540	243.570		243.565		243.560		243.555	1942.725	243.550		243.545
243.388	243.390	243.420		243.415		243.410	1956.282	243.405	1942.725	243.400		243.395

AFA2(LTT1, -2, -3, -4)	Round depth + 0.0 (mbsf)	AFA2(LTT1, -2, -3, -4) High	Depth - 0.5 cm (mbsf)	AFA1/2(LTT1, -2, -3, -4; TT1, -2, -3, -4) Match av	Depth - 1.5 cm (mbsf)	DC1/2 Match av	Depth - 1.5 cm (mbsf)	DC2a/DC2 Match av	Depth - 2.0 cm (mbsf)	DC2a/DC1 Match av	Depth - 2.5 cm (mbsf)	DC2 with high coherency
	244.760		244.755		244.750		244.745		244.740		244.735	
	244.610		244.605		244.600		244.595		244.590		244.585	
	244.460		244.455		244.450		244.445		244.440		244.435	
	244.300		244.295		244.290		244.285		244.280		244.275	
	244.150		244.145		244.140		244.135		244.130		244.125	
	244.000		243.995		243.990		243.985		243.980		243.975	
	243.850		243.845		243.840		243.835		243.830		243.825	
	243.690		243.685		243.680		243.675		243.670		243.665	
	243.540		243.535		243.530		243.525		243.520		243.515	
	243.390		243.385		243.380	2059.850	243.375		243.370		243.365	

Depth - 3.0 cm (mbsf)	DC2 pipe values	Combined depth (mbsf)	Combined values	Sort combined depth	Sort combined values	Clean combdepth
244.730		244.790		0.000		
244.580		244.640		0.005		
244.430		244.490		0.010		
244.270		244.330		0.015	2201.853	0.015
244.120		244.180		0.020		
243.970		244.030		0.025		
243.820		243.880		0.030		
243.660		243.720		0.035		
243.510		243.570		0.040		
243.360		243.420		0.130		

Notes: Combdepth = combined depth. Only a portion of this table appears here. The complete table is available in [ASCII format](#).

Table T3. Absolute depth shifts at Site 1103.

LDEO-BRG depth scale (mbsf)	Depth scale of unsynchronized data (mbsf)	Absolute depth shift (m)
7.630	81.865	5.765
102.413	98.915	3.498
108.052	106.515	1.537
131.826	130.965	0.861
142.037	141.315	0.722
162.763	165.065	2.302
165.354	167.465	2.111
167.335	169.715	2.38
195.986	197.515	1.529
207.569	210.565	2.996
210.007	216.115	6.108
212.598	220.365	7.767
229.819	230.065	0.246
233.934	232.665	1.269

Notes: To synchronize the new velocity data to other logging data of the Borehole Research Group at Lamont-Doherty Earth Observatory (LDEO-BRG), we used 14 prominent features of the IMPH resistivity log. The synchronization was achieved with the linear mode of AnalySeries 1.2 (Paillard et al., 1996). We consider the large depth shifts within the interval 207–212 mbsf as unrealistically high. Therefore, the correlation within this interval might be wrong.

Table T4. Final depth vs. velocity and two-way traveltime data.

Depth (mbsf)	Velocity (m/s)	TWT (s)	Depth (mbsf)	Velocity (m/s)	TWT (s)
0.00	1628.80	0.0000000	13.80	2111.95	0.0141548
0.20	1640.79	0.0002456	14.00	2111.95	0.0143442
0.40	1652.66	0.0004894	14.20	2111.95	0.0145336
0.60	1663.78	0.0007314	14.40	2111.95	0.0147230
0.80	1673.52	0.0009718	14.60	2111.96	0.0149124
1.00	1681.40	0.0012108	14.80	2111.96	0.0151018
1.20	1687.10	0.0014487	15.00	2111.96	0.0152912
1.40	1690.51	0.0016858	15.20	2111.96	0.0154806
1.60	1691.77	0.0019224	15.40	2111.96	0.0156700
1.80	1691.29	0.0021589	15.60	2111.96	0.0158594
2.00	1689.71	0.0023954	15.80	2111.97	0.0160488
2.20	1687.91	0.0026321	16.00	2111.97	0.0162382
2.40	1686.86	0.0028691	16.20	2111.97	0.0164276
2.60	1687.64	0.0031062	16.40	2111.97	0.0166170
2.80	1691.31	0.0033432	16.60	2111.97	0.0168064
3.00	1698.81	0.0035797	16.80	2111.97	0.0169958
3.20	1710.89	0.0038152	17.00	2111.98	0.0171852
3.40	1728.02	0.0040490	17.20	2111.98	0.0173746
3.60	1750.37	0.0042805	17.40	2111.98	0.0175640
3.80	1777.75	0.0045090	17.60	2111.98	0.0177534
4.00	1809.61	0.0047340	17.80	2111.98	0.0179428
4.20	1845.12	0.0049550	18.00	2111.99	0.0181322
4.40	1883.12	0.0051718	18.20	2111.99	0.0183216
4.60	1922.31	0.0053842	18.40	2111.99	0.0185110
4.80	1961.27	0.0055923	18.60	2111.99	0.0187003
5.00	1998.62	0.0057963	18.80	2111.99	0.0188897
5.20	2033.02	0.0059964	19.00	2111.99	0.0190791
5.40	2063.37	0.0061932	19.20	2112.00	0.0192685
5.60	2088.86	0.0063870	19.40	2112.00	0.0194579
5.80	2109.20	0.0065785	19.60	2112.00	0.0196473
6.00	2111.88	0.0067682	19.80	2112.00	0.0198367
6.20	2111.88	0.0069576	20.00	2112.60	0.0200261
6.40	2111.88	0.0071470	20.20	2113.42	0.0202154
6.60	2111.89	0.0073364	20.40	2114.12	0.0204047
6.80	2111.89	0.0075258	20.60	2114.62	0.0205939
7.00	2111.89	0.0077152	20.80	2114.87	0.0207831
7.20	2111.89	0.0079046	21.00	2114.85	0.0209722
7.40	2111.89	0.0080940	21.20	2114.57	0.0211614
7.60	2111.89	0.0082834	21.40	2114.08	0.0213505
7.80	2111.89	0.0084728	21.60	2113.44	0.0215397
8.00	2111.90	0.0086622	21.80	2112.74	0.0217290
8.20	2111.90	0.0088516	22.00	2112.06	0.0219183
8.40	2111.90	0.0090410	22.20	2111.49	0.0221077
8.60	2111.90	0.0092304	22.40	2111.07	0.0222971
8.80	2111.90	0.0094198	22.60	2110.87	0.0224866
9.00	2111.91	0.0096092	22.80	2110.88	0.0226761
9.20	2111.91	0.0097986	23.00	2111.10	0.0228656
9.40	2111.91	0.0099880	23.20	2111.50	0.0230551
9.60	2111.91	0.0101774	23.40	2112.01	0.0232445
9.80	2111.91	0.0103668	23.60	2112.60	0.0234339
10.00	2111.91	0.0105562	23.80	2113.15	0.0236233
10.20	2111.92	0.0107456	24.00	2113.62	0.0238126
10.40	2111.92	0.0109350	24.20	2113.96	0.0240018
10.60	2111.92	0.0111244	24.40	2114.13	0.0241910
10.80	2111.92	0.0113138	24.60	2114.12	0.0243802
11.00	2111.92	0.0115032	24.80	2113.93	0.0245694
11.20	2111.93	0.0116926	25.00	2113.61	0.0247586
11.40	2111.93	0.0118820	25.20	2113.18	0.0249479
11.60	2111.93	0.0120714	25.40	2112.71	0.0251372
11.80	2111.93	0.0122608	25.60	2112.25	0.0253265
12.00	2111.93	0.0124502	25.80	2111.86	0.0255159
12.20	2111.93	0.0126396	26.00	2111.58	0.0257053
12.40	2111.94	0.0128290	26.20	2111.44	0.0258947
12.60	2111.94	0.0130184			
12.80	2111.94	0.0132078			
13.00	2111.94	0.0133972			
13.20	2111.94	0.0135866			
13.40	2111.95	0.0137760			
13.60	2111.95	0.0139654			

Notes: The data are synchronized with the logging data of the Lamont-Doherty Earth Observatory Borehole Research Group. TWT = two-way traveltime. Only a portion of this table appears here. The complete table is available in [ASCII format](#).